JOURNAL OF MAGNETIC RESONANCE **125,** 291–301 (1997)
ARTICLE NO. MN971109

A Combination of Slow and Fast RF Field Modulation for Improved Cross Polarization in Solid-State MAS NMR

S. HEDIGER,* P. SIGNER,* M. TOMASELLI,* R. R. ERNST,* AND B. H. MEIER†

**Laboratorium für Physikalische Chemie, Eidgenössische Technische Hochschule, ETH-Zentrum, 8092 Zürich, Switzerland; and †NSR-Center for Molecular Structure, Design and Synthesis, Laboratory of Physical Chemistry, University of Nijmegen, Toernooiveld 6525 ED Nijmegen, The Netherlands*

Received December 11, 1996

A method for efficient Hartmann–Hahn cross polarization under rapid magic-angle sample spinning is presented. It combines rotor-synchronized amplitude modulation of one of the two spin-lock radio-frequency fields for dipolar recoupling, with a slow adiabatic amplitude variation to enhance the net polarization transfer. The proposed scheme, called AMAP-CP, allows for cross polarization on the original Hartmann–Hahn matching condition $\omega_{1I} = \omega_{1S}$. The polarization transfer is insensitive to chemical-shift offsets, rotation frequency, and inhomogeneity of the radiofrequency field.

1. INTRODUCTION

Heteronuclear polarization transfer by cross polarization (CP) is widely used to improve the sensitivity of NMR for spins with low gyromagnetic ratio or for heteronuclear correlation experiments. The most popular technique for cross polarization is Hartmann–Hahn cross polarization (HHCP) (*1–3*) where the abundant spins I with high gyromagnetic ratio (e.g., protons) are brought in contact with the insensitive spins S (e.g., ^{13}C or ^{15}N) by applying spin-lock radiofrequency fields with amplitudes B_{1I} and B_{1S}. For efficient transfer, the amplitudes of the spin-lock fields must be matched at the Hartmann–Hahn condition $\omega_{1I} = \omega_{1S}$ (in a static or slowly rotating sample), with $\omega_{1I} = -\gamma_I B_{1I}$ and $\omega_{1S} = -\gamma_S B_{1S}$.

The effect of high-speed magic-angle spinning (MAS) on Hartmann–Hahn CP was first investigated by Stejskal *et al.* (*3*). The dipolar couplings are modulated with the MAS frequency ω_r and with $2\omega_r$. When ω_r exceeds the dipolar coupling frequencies, new modified Hartmann–Hahn matching conditions appear, offset by integers of the rotation frequency, $\omega_{1I} - \omega_{1S} = \pm n\omega_r$, $n = 1, 2, 3, \ldots$. The new matching conditions are usually much narrower than the Hartmann–Hahn condition in static samples, and their matching requires rather stable and homogeneous RF field amplitudes and stable MAS rotation frequencies. The transfer rate at the original Hartmann–Hahn condition, $\omega_{1I} = \omega_{1S}$, and at higher sidebands of the Hartmann–Hahn condition ($n > 2$) tends toward zero with increasing spinning frequency (*4, 5*). Although the Hartmann–Hahn transfer at the exact sideband matching conditions $\omega_{1I} - \omega_{1S} = \pm\omega_r$ or $\pm 2\omega_r$ can be quite efficient, it is not well suited for practical applications because of its sensitivity to RF field inhomogeneity and to the MAS frequency.

A number of pulse sequences were proposed in the past to improve cross polarization under MAS conditions. They pursue three goals:

(i) Efficient polarization transfer at the original Hartmann–Hahn centerband matching condition $\omega_{1I} = \omega_{1S}$. Rotor-synchronized amplitude modulation (AMCP) (*6, 7*) reintroduces a time-independent dipolar-coupling element and allows cross polarization for $\omega_{1I} = \omega_{1S}$. The matching condition is independent of the spinning speed and, for a single-coil probe, of the RF inhomogeneity. An alternative method for centerband matching is to prevent the MAS averaging of the dipolar interaction by limiting the cross-polarization process to a fraction of the rotor periods (*8*). Other sequences that restore the heteronuclear dipolar interaction were proposed for distance measurements in recoupled spectra (*9–16*).

(ii) Broadening of the matching conditions for less critical matching of the RF field amplitudes. The matching conditions can be broadened by phase modulation that reduces the average spin-lock field, either by rotor-synchronized 180° phase modulation alone as in SPICP (*17–19*) or in combination with amplitude modulation (AMCP) (*7*). Alternatively, uncertainties in the Hartmann–Hahn matching condition, such as inaccurate RF field amplitudes or RF field inhomogeneity, can be coped with by using a variable RF field amplitude (VACP, RAMP-CP) (*20–22*), 180° phase shifts (VEFCP) (*23*), or a frequency sweep (*24*). The broadening of the matching condition by a multiple-pulse approach was proposed by Geen *et al.* (*25*).

(iii) Optimization of the quasi-equilibrium polarization transfer. The polarization transfer after a long cross-polarization period can be enhanced by an adiabatic sweep of the

1090-7807/97 $25.00

RF field amplitude through the Hartmann–Hahn condition (APHH-CP). This leads, in isolated two-spin systems which do not benefit from rapid spin diffusion among the protons, to a net polarization transfer enhanced by up to a factor two. The factor two comes from a complete adiabatic polarization transfer from the I to the S spin compared to the equidistribution of the polarization in a standard Hartmann–Hahn experiment (*26*). This was demonstrated for static (*26, 27*) as well as for rotating samples (*28–31*). Under MAS, the adiabatic sweep had to be performed so far on a sideband-matching condition.

We present in the following a new pulse scheme that reaches simultaneously all three goals: (i) efficient centerband cross polarization, (ii) broadening of the Hartmann–Hahn matching condition, and (iii) enhanced quasi-equilibrium polarization.

2. THE PULSE SEQUENCE AMAP-CP

The proposed pulse sequence, called AMAP-CP (*a*mplitude-*m*odulated *a*diabatic-*p*assage *CP*), combines amplitude-modulated cross polarization (AMCP) with adiabatic-passage Hartmann–Hahn cross polarization (APHH-CP) as is shown in Fig. 1. The fast rotor-synchronized amplitude modulation of AMCP (Fig. 1a) is known to cause efficient dipolar recoupling of the I and S spins (*7*), and leads to a strongly accelerated cross-polarization process. It was found in Ref. (*7*) that a cosine amplitude modulation with the MAS frequency ω_r and with the amplitude 2.1 ω_r or its square-wave approximation with amplitude $\pm 1.65\ \omega_r$, as illustrated in Fig. 1a, yields a cross-polarization rate close to its theoretical maximum for centerband matching.

The combination with a slow adiabatic passage through the Hartmann–Hahn condition (Fig. 1b) renders the polarization transfer insensitive to an exact match of the RF field strengths and allows simultaneously an enhancement of the quasi-equilibrium polarization transfer (*29*). Adiabatic passage CP is particularly effective for virtually isolated IS spin systems as they occur typically for ^{1}H–^{13}C, ^{1}H–^{15}N, or ^{15}N–^{13}C pairs under fast MAS conditions when I-spin diffusion is quenched.

The combination of the two schemes is feasible without major difficulties, leading to the proposed sequence AMAP-CP. The two amplitude-modulation functions could be applied to two different RF channels, e.g., the square-wave or sine-wave modulation to the I-spin (^{1}H) channel and the adiabatic passage to the S-spin (^{13}C) channel. In the version of Fig. 1c, it was decided, for convenience, to apply both modulation functions simultaneously to the S channel. A constant RF field strength on the I spins ensures good spin-lock properties for the entire mixing time, limiting in this way the loss due to $T_{1\rho}(^1\mathrm{H})$ relaxation.

It was shown in Ref. (*29*) that an efficient transfer is

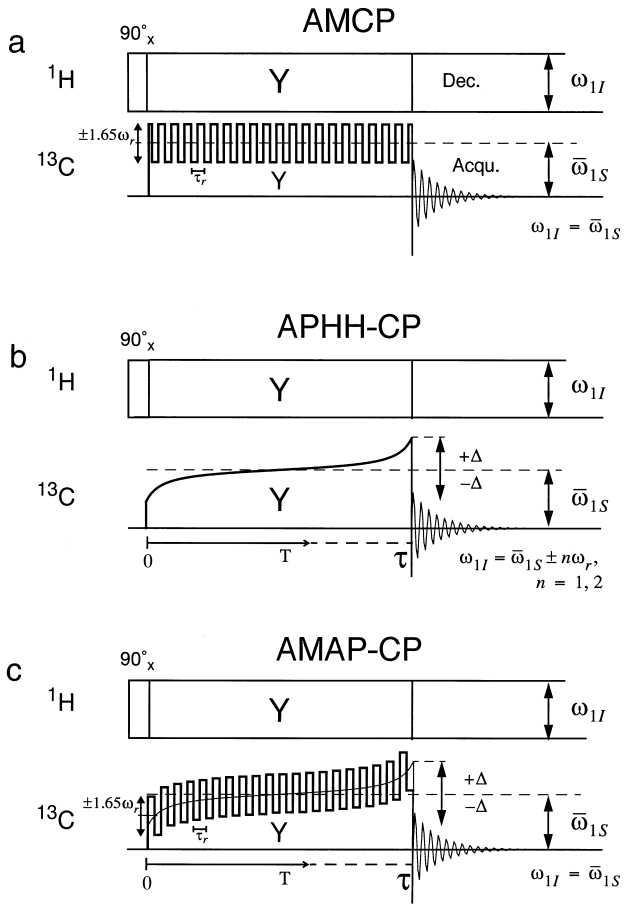

FIG. 1. Pulse sequences for (a) rotor-synchronized amplitude-modulated cross polarization (AMCP) (*7*), (b) adiabatic-passage Hartmann–Hahn cross polarization (APHH-CP) under MAS at a sideband matching condition (*29*), and (c) amplitude-modulated adiabatic-passage cross polarization (AMAP-CP) at the centerband matching condition. $\tau_r = \omega_r/2\pi$ represents the MAS period.

obtained when the adiabatic passage follows a tangent function of the form

$$\omega_{1I}^{(0)}(T) - \omega_{1S}^{(0)}(T) = |D_0| \tan[\alpha_0(\tfrac{1}{2}\tau - T)], \qquad [1]$$

for $0 \leqslant T \leqslant \tau$, with

$$\alpha_0 = \frac{2}{\tau} \arctan\left(\frac{\Delta}{|D_0|}\right), \qquad [2]$$

where 2Δ represents the amplitude of the tangential sweep through the Hartmann–Hahn condition with $-\Delta \leqslant \omega_{1I}^{(0)}(T) - \omega_{1S}^{(0)}(T) \leqslant \Delta$. D_0 is the time-independent dipolar coupling reintroduced by the AMCP part of the modulation (see Appendix 1), and $\omega_{1I}^{(0)}(T)$ and $\omega_{1S}^{(0)}(T)$ are the mean RF field strengths of the AMCP modulation averaged over

one rotor period. To prevent interference with the sideband HH matching, the condition $\Delta < \omega_r/2$ should be fulfilled.

As described in Ref. (*26*), the tangential time dependence of Eq. [1] leads to a circular trajectory of the density operator, at constant angular frequency $(d/dt)\theta_0^{\Delta} = \alpha_0$, on a half-circle in the two-dimensional zero-quantum subspace spanned by I_z^{Δ} and I_x^{Δ} (Eq. [A5]). A complete passage results in an inversion of the difference polarization if the adiabatic condition (*32, 33*) $(d/dT)\theta_0^{\Delta} \ll \sqrt{[\omega_{1I}^{(0)}(T) - \omega_{1S}^{(0)}(T)]^2 + D_0^2}$ is fulfilled, and if the angle $\theta_0^{\Delta}(T = 0)$ between the initial density operator along the z axis and the quantization axis of the Hamiltonian at $T = 0$ is small. To fulfill this last condition, the amplitude difference between the mean fields at $T = 0$, $\Delta = \omega_{1I}^{(0)}(0) - \omega_{1S}^{(0)}(0)$, must be larger than the dipolar coupling, $\Delta \gg D_0$, while still $\Delta < \omega_r/2$. This is only possible for rapid spinning, $\omega_r \gg d_{IS}$.

A proper choice of the sweep time τ and amplitude 2Δ of the adiabatic passage (Eqs. [1] and [2]) requires an estimate of the coupling element $|D_0|$. For the optimized AMCP sequences used here, the mean coupling element $|\overline{D_0}|$ (where the bar denotes the powder average) is about 5 times smaller than the dipolar coupling constant d_{IS}. This can be seen from Fig. 2 where the dipolar coupling elements $|\overline{D_n}|$ are plotted for the optimized cosine modulation and its square-wave approximation. They are analytically given by Eq. [27] of Ref. (*7*) and have been computed here by numerically performing the Floquet matrix transformation described in Ref. (*7*).

For the optimum functioning of the AMAP-CP pulse sequence (see Appendix 1), it is necessary that the transfer, driven by a flip–flop Hamiltonian, is restricted to the zero-quantum subspace. This can be achieved by the use of sufficiently strong RF fields and rapid spinning $|\omega_{1I} + \omega_{1S}| \gg \omega_r > d_{IS}$. The double-quantum flop–flop term is then nonsecular, and the sum polarization can be considered as a constant of the motion. The presence of the AMCP modulation may cause additional problems. The modulation introduces higher-order Fourier coupling elements D_n, given by Eq. [27] in Ref. (*7*), which must be considered typical for n up to 7 or 8 as can be inferred from Figs. 2a and 2b for the optimized cosine modulation and its square-wave approximation. These coupling elements can, possibly, induce flop–flop spin transitions when the sideband conditions $\omega_{1I}^{(0)}(T) + \omega_{1S}^{(0)}(T) = n\omega_r$ are fulfilled, as described in Ref. (*4*). These double-quantum transitions lead, for longer contact times, to a decay of the sum polarization and of the detected S-spin signal. In AMAP-CP experiments, the RF fields should therefore be strong enough ($\omega_{1I} + \omega_{1S} > 8\omega_r$) to avoid the destructive double-quantum matching conditions. Because the higher-order coupling elements $|\overline{D_n}|$ are (for the same n) slightly smaller for the optimized cosine modulation than for its square-wave approximation (see Fig. 2), the cosine modulation is preferable.

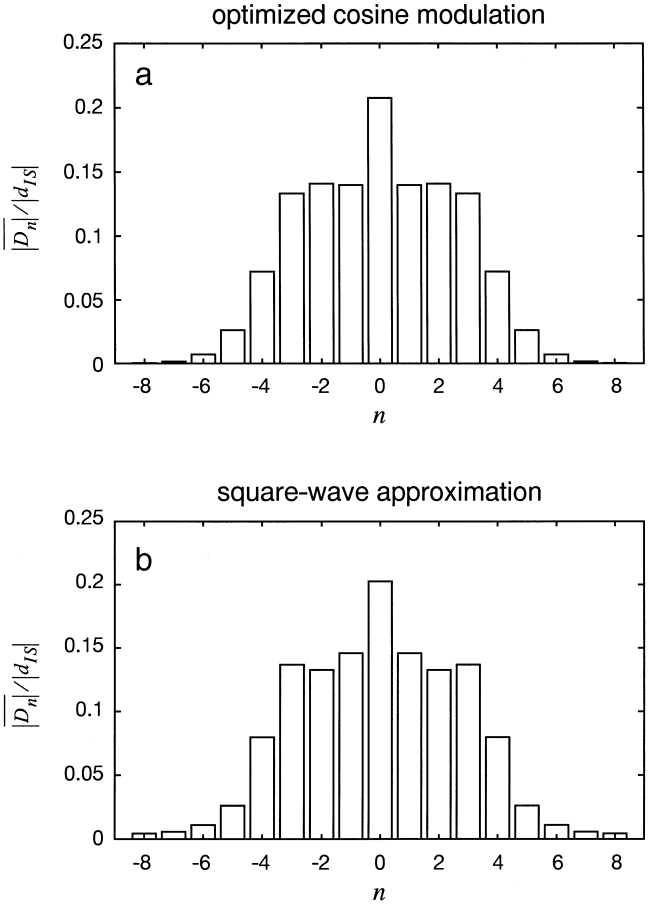

FIG. 2. Effective Fourier coefficients $|\overline{D_n}|$ of the dipolar coupling, normalized by the dipolar interaction $|d_{IS}|$ and averaged over 986 crystallite orientations (a) for the optimum cosine modulation (*7*) of frequency ω_r and amplitude 2.1 ω_r, and (b) for its square-wave approximation depicted in Fig. 1a with amplitude $\pm 1.65\ \omega_r$ around the centerband matching condition. The coupling elements were obtained by numerically performing the Floquet matrix transformation described in Ref. (*7*).

3. EXPERIMENTAL RESULTS

The AMAP-CP pulse sequence was first tested on a powder sample of crystalline C_{60}(ferrocene)$_2$ (*34*). For determining the width of the tangential sweep according to Eqs. [1] and [2], the coupling element $D_0/2\pi$ was assumed to be 5 kHz. Due to the fast rotation (on the NMR scale) of the C_5H_5 rings in ferrocene, the homonuclear and heteronuclear intraring dipolar interactions are scaled by a factor 2, and the interring interactions are also reduced. The suppression of the dipolar interactions by fast MAS is then quite effective. In the presence of a heteronuclear recoupling sequence, like AMCP, the ferrocene ^{13}C spins with their directly bound protons form fairly well-isolated two-spin pairs. The effective heteronuclear coupling frequency is much larger than the remaining homonuclear proton couplings. Therefore, an adiabatic intensity gain of two is expected in an AMAP-CP experiment (see Appendix 1).

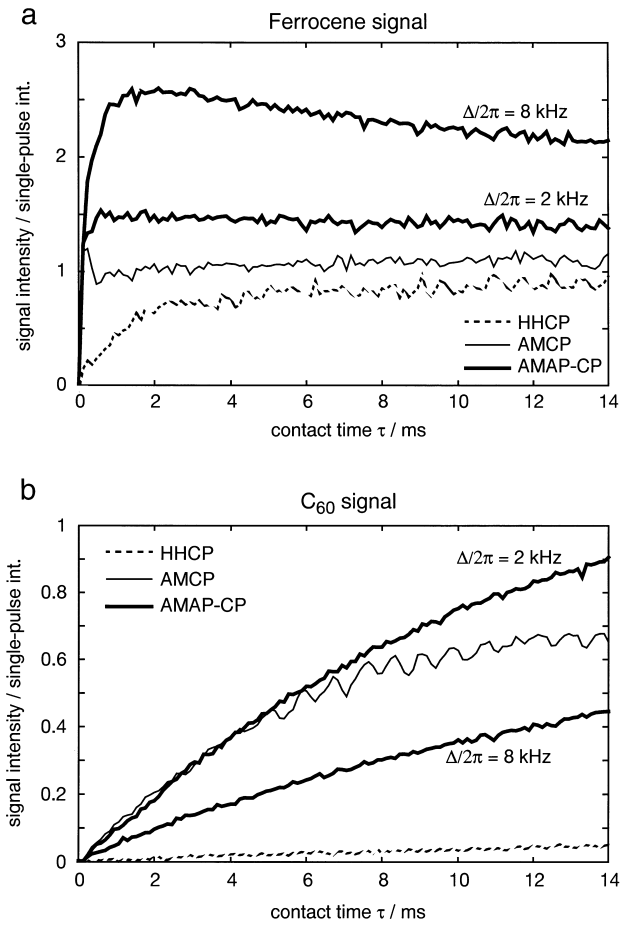

FIG. 3. Cross polarization in polycrystalline C_{60}(ferrocene)$_2$ using HHCP, AMCP, and AMAP-CP. The signal intensity, normalized by the signal intensity obtained with a single ^{13}C pulse, is given as a function of the mixing time τ. The RF field strengths were set to 74 kHz and the MAS frequency was 17 kHz. Tangent depths $\Delta/2\pi$ of 2 and 8 kHz were used. (a) Ferrocene ^{13}C signal, and (b) C_{60} ^{13}C signal.

The C_{60} carbons, in contrast, are only weakly coupled to the many protons on the neighboring ferrocene molecules, and the heteronuclear couplings will remain weak and comparable to the homonuclear proton couplings. During the long cross-polarization times necessary, spin diffusion among the proton spins will be quite effective and the theoretical advantage of AMAP-CP in comparison to AMCP for centerband matching or HHCP for sideband matching will be minimal. However, due to the small size of the heteronuclear couplings, it becomes difficult to match the Hartmann–Hahn condition in HHCP or AMCP experiments, and a mismatch due to RF field inhomogeneity effects will reduce the cross-polarization rate. In this respect the mismatch-insensitive Hartmann–Hahn matching of AMAP-CP is of advantage.

In Fig. 3, the S-spin polarization buildup for the two carbon resonances in C_{60}(ferrocene)$_2$ is compared for HHCP, AMCP, and AMAP-CP. The experiments were performed at a MAS frequency of 17 kHz, and the mean RF field strengths for Hartmann–Hahn centerband matching were set to 74 kHz. As expected, the AMCP buildup proceeds significantly faster than the HHCP buildup for both resonances. A substantial improvement of the maximum signal amplitude is obtained with the AMAP-CP scheme. For ferrocene, the AMAP-CP signal is, for short contact periods, equal and, for longer contact ($>$0.1 ms), larger than the AMCP signal. For $\Delta/2\pi = 8$ kHz, the intensity reaches its maximum value at a contact time of $\sim$2 ms. It is 2.5 times larger than the asymptotic value for AMCP, exceeding the theoretically expected gain of 2 for a two-spin system. This can be explained by the improved compensation of the RF field inhomogeneity and of the chemical-shift offset effects by the adiabatic passage. It is apparent that the intensity of the AMAP-CP signal at longer mixing times decreases more rapidly than expected from the $T_{1\rho}$ value determined in a CW spin-lock experiment ($T_{1\rho} > 100$ ms). We attribute this enhanced decay to flop–flop transitions. In the experiment of Fig. 3, the RF field is close to the resonance condition $\omega_{1I} + \omega_{1S} = 9\omega_r$ that would be met at $\omega_{1S}/2\pi = 79$ kHz. Such effects can also be seen in AMCP experiments (unpublished results). They are expected to become stronger at lower ratios of RF field amplitude to spinning speed.

Although the relative intensities obtained with the different CP methods are qualitatively consistent with the theory, a comparison with the intensity obtained after a 90° pulse applied to the carbons shows that the net polarization enhancement is significantly less than expected from the gyromagnetic ratios. The theoretical gain in quasi-equilibrium polarization P_S obtained in a HHCP experiment in comparison to the Zeeman polarization of the S spin P_{0S} is given, for equal spin quantum numbers I = S, by $P_S/P_{0S} = (\gamma_I/\gamma_S)\cdot N_I/(N_I + N_S)$, where N_I and N_S are the number of I and S spins, respectively (*2*). For an isolated two-spin ^1H–^{13}C system, a gain of 2 for HHCP (sideband matching) or AMCP (centerband matching) and of 4 for AMAP-CP is expected compared to that of the single-pulse experiment. In all our cross-polarization experiments under MAS, the intensities are about a factor 1.5 lower than the theoretical expectations. The reason for this loss is not clear. The loss of polarization seems to increase by using higher spin-lock power and higher MAS frequencies, and we suspect that it could be caused by increasing instabilities of the RF fields, which could become critical in the high-speed MAS regime.

For cross polarization of C_{60} in C_{60}(ferrocene)$_2$, Fig. 3b, where no adiabatic gain is expected, a small improvement of the cross-polarization efficiency by AMAP-CP compared to AMCP was observed when a small tangent depth ($\Delta/2\pi = 2$ kHz) was used. We attribute this gain to the compensation of the RF inhomogeneity. With larger tangent depths, the buildup rate is slowed down because during an increasing fraction of the contact time, the Hartmann–Hahn condition is violated.

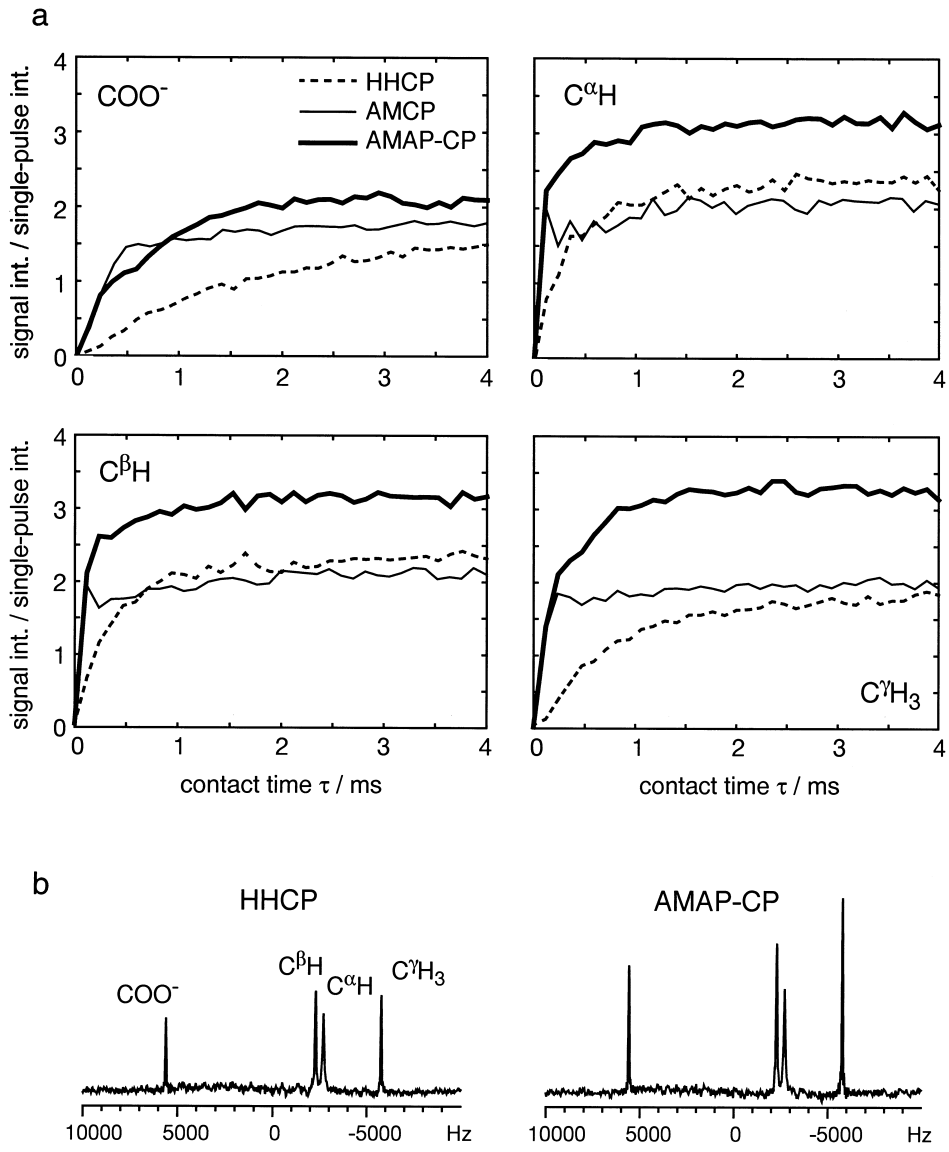

FIG. 4. (a) Cross polarization in polycrystalline L-threonine using HHCP, AMCP, and AMAP-CP as a function of the mixing time τ. The RF field strengths $\omega_{1I}/2\pi$ and $\overline{\omega}_{1S}/2\pi$ were set to 72 kHz and the MAS frequency to 17 kHz. A tangent depth $\Delta/2\pi = 8$ kHz was used for the AMAP-CP pulse sequence. The intensities are given in units of the intensity obtained with a single-pulse experiment. (b) L-Threonine spectra after 2 ms contact time using HHCP and AMAP-CP under the same condition as in (a). Sixteen scans were added.

HHCP and AMAP-CP signal intensities were also compared for a sample of L-threonine. Threonine shows little motion in the solid state and exhibits strong hetero- and homonuclear dipolar couplings. The spinning frequency of 17 kHz does not exceed the proton–proton dipolar couplings. Nevertheless, the CP matching profile (not shown) decomposes into a set of spinning sidebands. Also in this sample, AMAP-CP leads to considerable intensity gains as shown in Fig. 4 where the intensities of the four carbon resonances are given as functions of the contact time for HHCP, AMCP, and AMAP-CP. The proton RF field strength was set to 72 kHz. The intensities of the buildup curves are again normalized by the corresponding signal intensity obtained with a single-pulse experiment. HHCP and AMCP lead, for longer contact times, to comparable quasi-equilibrium polarizations for all resonances. A gain of a factor two over the equilibrium carbon polarization is achieved. The buildup rates are considerably faster for AMCP. The intensity gain obtained with AMAP-CP amounts to 33% for the CH groups and 75% for the CH_3 group, compared to HHCP or AMCP. No adiabatic enhancement was observed for the carboxylic resonance, in analogy to the observation for C_{60}.

4. CONCLUSIONS

It has been demonstrated that adiabatic polarization transfer under high-speed MAS is possible at the rotor-frequency-independent Hartmann–Hahn centerband condition when an adiabatic sweep of the RF field amplitude is combined with a rotor-synchronized amplitude modulation. The latter reintroduces a secular dipolar coupling element between I and S spins at the centerband matching condition. Due to the different time scales of the two amplitude variations, the combination of the adiabatic-passage and amplitude-modulation schemes is free of interferences.

AMAP-CP combines fast polarization transfer at the centerband of the Hartmann–Hahn condition, as in AMCP, with an equilibrium-intensity gain due to the adiabatic transfer, as observed in the APHH-CP experiment. Matching at a rotor-frequency-dependent sideband condition, necessary with earlier adiabatic methods under MAS (*29*), can be avoided. As usual, the adiabatic sweep broadens the matching condition and renders it less sensitive to RF field inhomogeneities, chemical-shift offsets, and long-term instabilities of the RF amplifiers.

Adiabatic cross-polarization transfer is of particular advantage for relatively isolated spin systems, e.g., IS spin pairs. Such spin pairs occur for double isotopic labeling, e.g., in $^{13}C-^{15}N$-labeled compounds (*30*) or, dynamically, by high-speed MAS through the averaging of proton–proton interactions. With the development of faster spinning probes, adiabatic cross polarization is expected to become increasingly advantageous. But even below the fast spinning regime, substantial intensity gains are obtained, as shown by the experiments on L-threonine.

APPENDIX 1

Theoretical Treatment of AMAP-CP

We develop in this Appendix a theoretical description of the AMAP-CP experiment that takes advantage of the different time scales of the two amplitude variation. Their effect on polarization transfer can be understood by first considering the effect of the ''fast'' modulation and, in a second step, the effect of the ''slow'' adiabatic variation under an average Hamiltonian determined by the fast amplitude modulation. For the description of the AMCP effect, we apply here average-Hamiltonian theory rather than Floquet theory that has been used in Ref. (*7*). At the end of Appendix 1, the equivalence of the two approaches is demonstrated.

We consider here a heteronuclear two-spin system (IS) of spin-$\frac{1}{2}$ nuclei. The Hamiltonian in a tilted doubly rotating frame and for amplitude-modulated on-resonance RF fields of strengths $\omega_{1I}(t, T)$ and $\omega_{1S}(t, T)$ can be written as

$$\mathcal{H}(t, T) = \omega_{1I}(t, T)I_z + \omega_{1S}(t, T)S_z + 2b(t)I_yS_y, \quad [A1]$$

with

$$b(t) = \sum_{n=-2}^{+2} b_n \exp(in\omega_r t) \quad [A2]$$

and with the Fourier components of the dipolar coupling

$$b_{\pm 1} = -\frac{d_{IS}}{2\sqrt{2}} \sin(2\theta)\exp(\pm i\varphi),$$

$$b_{\pm 2} = \frac{d_{IS}}{4} \sin^2\theta \exp(\pm 2i\varphi). \quad [A3]$$

Here $d_{IS} = -\mu_0\gamma_I\gamma_S\hbar/(4\pi r_{IS}^3)$ represents the dipolar coupling constant in angular frequency units, and θ and φ are the polar angles of the internuclear vector $\mathbf{r}_{IS}$ in a MAS rotor-fixed coordinate system. We distinguish a ''slow-time variable'' T, arising from the adiabatic sweep of the RF amplitude, and a ''fast-time variable'' t, responsible for the rotor-synchronized AMCP part of the field modulation and for the time dependence of the dipolar interaction. As usual, this Hamiltonian can be decomposed into double-quantum (Σ) and zero-quantum (Δ) contributions:

$$\mathcal{H}(t, T) = \mathcal{H}^{\Sigma}(t, T) + \mathcal{H}^{\Delta}(t, T),$$
$$\mathcal{H}^{\Sigma}(t, T) = [\omega_{1I}(t, T) + \omega_{1S}(t, T)]I_z^{\Sigma} - b(t)I_x^{\Sigma},$$
$$\mathcal{H}^{\Delta}(t, T) = [\omega_{1I}(t, T) - \omega_{1S}(t, T)]I_z^{\Delta} + b(t)I_x^{\Delta}, \quad [A4]$$

with the single-transition operators (*37–39*)

$$I_x^{\Sigma} = \tfrac{1}{2}[I^+S^+ + I^-S^-], \quad I_y^{\Sigma} = \frac{-i}{2}[I^+S^+ - I^-S^-],$$
$$I_z^{\Sigma} = \tfrac{1}{2}[I_z + S_z], \quad I_x^{\Delta} = \tfrac{1}{2}[I^+S^- + I^-S^+],$$
$$I_y^{\Delta} = \frac{-i}{2}[I^+S^- - I^-S^+], \; I_z^{\Delta} = \tfrac{1}{2}[I_z - S_z]. \quad [A5]$$

For strong RF fields and rapid spinning ($|\omega_{1I} + \omega_{1S}| \gg \omega_r > d_{IS}$), the polarization transfer takes place predominantly in the zero-quantum subspace and the discussion can be restricted to $\mathcal{H}^{\Delta}$. The validity of this assumption was discussed at the end of Section 2.

Because the adiabatic sweep, represented by the time variable T, is much slower than the AMCP amplitude modulation, the latter can be treated in the presence of a constant mean RF field that depends on the parameter T. This shall be symbolized by the writing

$$\mathcal{H}_T^{\Delta}(t) = [\omega_{1I}(t) - \omega_{1S}(t)]_T I_z^{\Delta} + b(t)I_x^{\Delta}. \quad [A6]$$

The modulation of the RF field-strength difference $[\omega_{1I}(t) - \omega_{1S}(t)]_T$ can be expressed by a series of cosine functions up to the arbitrarily limited order N:

$$[\omega_{1I}(t) - \omega_{1S}(t)]_T = [\omega_{1I}^{(0)} - \omega_{1S}^{(0)}]_T + \sum_{l=1}^{N} a^{(l)}\cos(l\omega_r t + \phi_l). \quad [A7]$$

The Hamiltonian of Eq. [A6], together with Eq. [A7], describes a rotor-synchronized amplitude-modulated CP scheme (AMCP) that was discussed in Ref. (*7*). Using a Floquet approach, the features of AMCP were derived in an interaction frame with the same time dependence as the RF amplitudes. The calculation can also be done in Liouville space by considering the offset term $[\omega_{1I}^{(0)} - \omega_{1S}^{(0)}]_T I_z^{\Delta}$ and the dipolar contribution $b(t)I_x^{\Delta}$ as the relevant parts of the Hamiltonian, $\mathcal{H}_{T0}^{\Delta}$, and the modulated part of the RF fields as a perturbation which can be eliminated by a transformation into an interaction frame (*39*)

$$\tilde{\mathcal{H}}_T^{\Delta}(t) = \mathbf{U}_1^{-1}(t) \cdot \mathcal{H}_{T0}^{\Delta} \cdot \mathbf{U}_1(t), \quad [A8]$$

with

$$\mathcal{H}_{T0}^{\Delta} = [\omega_{1I}^{(0)} - \omega_{1S}^{(0)}]_T I_z^{\Delta} + b(t) I_x^{\Delta}$$

and

$$\mathbf{U}_1(t) = \exp\left\{ -i \int_0^t [\sum_{l=1}^{N} a^{(l)}\cos(l\omega_r t_1 + \phi_l)] I_z^{\Delta} dt_1 \right\}. \quad [A9]$$

The propagator $\mathbf{U}_1(t)$ describes a rotation of variable speed around the z axis of the tilted rotating frame with the phase angle $\theta(t)$:

$$\theta(t) = \int_0^t \sum_{l=1}^{N} a^{(l)}\cos(l\omega_r t_1 + \phi_l) dt_1 = \sum_{l=1}^{N} \frac{a^{(l)}}{l\omega_r} [\sin(l\omega_r t + \phi_l) - \sin(\phi_l)]. \quad [A10]$$

By expanding the trigonometric functions into Bessel functions, using the relation $\exp\{iz \sin \Phi\} = \sum_{k=-\infty}^{\infty} \exp\{ik\Phi\} \cdot J_k(z)$, we find that

$$\tilde{\mathcal{H}}_T^{\Delta}(t) = [\omega_{1I}^{(0)} - \omega_{1S}^{(0)}]_T I_z^{\Delta} + \mathrm{Re}\{D(t)\} I_x^{\Delta} - \mathrm{Im}\{D(t)\} I_y^{\Delta}. \quad [A11]$$

The dipolar coupling element $D(t)$ in the interaction frame is given by

$$D(t) = \exp\{iA\} \cdot b(t) \prod_{l=1}^{N} \sum_{k_l=-\infty}^{\infty} J_{k_l}\left(\frac{a^{(l)}}{l\omega_r}\right) \times \exp\{ik_l l\omega_r t\} \cdot \exp\{ik_l \phi_l\}, \quad [A12]$$

where the overall phase factor $\exp\{iA\}$ is defined by $A = -\sum_{l=1}^{N} a^{(l)}\sin(\phi_l)/(l\omega_r)$. For a spinning speed much larger than the heteronuclear dipolar coupling d_{IS}, and a sweep width limited to the centerband matching region, $|[\omega_{1I}^{(0)} - \omega_{1S}^{(0)}]_T| \leqslant \omega_r/2$, the interaction frame used above is appropriate for the entire adiabatic-passage process with the time variable T. The zero-order average Hamiltonian (*40, 41*), approximating the time-dependent Hamiltonian of Eq. [A11], contains only the time-independent dipolar-coupling element D_0 and is given by

$$\bar{\mathcal{H}}^{\Delta}(T) = [\omega_{1I}^{(0)} - \omega_{1S}^{(0)}]_T I_z^{\Delta} + \mathrm{Re}\{D_0\} I_x^{\Delta} - \mathrm{Im}\{D_0\} I_y^{\Delta}. \quad [A13]$$

Using Eq. [A12] and Eqs. [A2] and [A3], D_0 is found to be

$$D_0 = \exp\{iA\} \sum_{n=-2}^{+2} b_n \sum_{k_2=-\infty}^{\infty} \cdots \sum_{k_N=-\infty}^{\infty} J_{-n-2k_2-\cdots-Nk_N}\left(\frac{a^{(1)}}{\omega_r}\right) \times J_{k_2}\left(\frac{a^{(2)}}{2\omega_r}\right) \cdots J_{k_N}\left(\frac{a^{(N)}}{N\omega_r}\right) \times \exp\{i(-n - 2k_2 - \cdots - Nk_N)\phi_1\} \times \exp\{ik_2\phi_2\} \cdots \exp\{ik_N\phi_N\}. \quad [A14]$$

This is the desired final result. Because $D(t)$ is complex, the dipolar interaction expressed by D_0 is no longer along the x axis of the zero-quantum subspace but contains also a contribution along y. However, the initial density operator as well as the detection operator commute with a zero-quantum frame z rotation, and we can rotate the interaction frame around the z axis such that D_0 becomes real. The Hamiltonian of Eq. [A13] is then identical to the static APHH-CP Hamiltonian of Ref. (*26*). In full analogy, an adiabatic polarization transfer is possible if the average RF field amplitude $[\omega_{1I}^{(0)} - \omega_{1S}^{(0)}]_T$ is slowly swept through the Hartmann–Hahn condition according to the tangent function given in Eq. [1]. Inside a two-spin system, the polarization is then completely transferred from the I to the S spin, leading to a net polarization enhanced by a factor two compared to the standard HHCP.

We derive in the following the equivalence of the expression for D_0, Eq. [A14], obtained here with average Hamilto-

nian theory, with the corresponding expression, Eq. [28] of Ref. (*7*), derived by Floquet theory. In Ref. (*7*), the dipolar coupling element D_0 was obtained as (Eq. [28])

$$D_0 = b_1 \sum_{s=-\infty}^{\infty} \delta_{-s}\delta_{s-1} + b_{-1} \sum_{s=-\infty}^{\infty} \delta_{-s}\delta_{s+1} + b_2 \sum_{s=-\infty}^{\infty} \delta_{-s}\delta_{s-2} + b_{-2} \sum_{s=-\infty}^{\infty} \delta_{-s}\delta_{s+2}, \qquad [A15]$$

where the δ_f denotes the elements of the transformation matrix found by solving the eigenvalue problem of the RF Floquet Hamiltonian [Eq. [23] of Ref. (*7*)]:

$$\begin{aligned}\delta_f = [\sum_{k_1=-\infty}^{\infty} \sum_{k_2=-\infty}^{\infty} \cdots \sum_{k_{N-1}=-\infty}^{\infty} & J_{f-2k_1-3k_2-\cdots-Nk_{N-1}}(-X_1) \\ & \times J_{k_1}(-X_2)\cdot J_{k_2}(-X_3)\cdot \ldots \cdot J_{k_{N-1}}(-X_N) \\ & \times \exp\{i(f - 2k_1 - 3k_2 - \cdots - Nk_{N-1})\phi_1\} \\ & \times \exp\{ik_1\phi_2\}\cdot\exp\{ik_2\phi_3\}\cdot \ldots \\ & \times \exp\{ik_{N-1}\phi_N\}]\exp\left\{\frac{iB}{2}\right\}. \end{aligned} \qquad [A16]$$

The terms δ_f are defined only up to a phase factor $\exp\{iB/2\}$ that can be chosen at will and was set to 1 in Ref. (*7*). In Eq. [A16], X_n defines the normalized amplitudes

$$X_n = \frac{|\omega_{1S}^{(n)} - \omega_{1I}^{(n)}|}{n\omega_r}, \qquad [A17]$$

and ϕ_n the phases

$$\phi_n = \arg(\omega_{1S}^{(n)} - \omega_{1I}^{(n)}) \qquad [A18]$$

of the Fourier coefficients of the RF modulation

$$\begin{aligned}\omega_{1S}(t) - \omega_{1I}(t) &= \sum_{n=-N}^{N} (\omega_{1S}^{(n)} - \omega_{1I}^{(n)})\cdot\exp\{in\omega_r t\} \\ &= \sum_{n=0}^{N} 2|\omega_{1S}^{(n)} - \omega_{1I}^{(n)}| \\ &\quad \times \cos(n\omega_r t + \phi_n). \end{aligned} \qquad [A19]$$

By comparing this equation with Eq. [A7] of this contribution, we get the following relationship between the cosine amplitude coefficients $a^{(n)}$, $n = 1 \ldots N$, and the normalized coefficients X_n:

$$X_n = \frac{-a^{(n)}}{2n\omega_r}. \qquad [A20]$$

Using the property of the Bessel functions $\Sigma_{k=-\infty}^{\infty} J_k(z)J_{n-k}(z) = J_n(2z)$, Eq. [A15] can be rewritten as

$$\begin{aligned}D_0 = [\sum_{n=-2}^{2} b_n \sum_{l_1=-\infty}^{\infty} \cdots \sum_{l_{N-1}=-\infty}^{\infty} \sum_{m_1=-\infty}^{\infty} \cdots \sum_{m_{N-1}=-\infty}^{\infty} & J_{-n-2(l_1+m_1)-3(l_2+m_2)-\cdots-N(l_{N-1}+m_{N-1})}(-2X_1) \\ & \times J_{l_1+m_1}(-2X_2)\cdot J_{l_2+m_2}(-2X_3)\cdot \ldots \\ & \times J_{l_{N-1}+m_{N-1}}(-2X_N)\exp\{i[-n - 2(l_1 + m_1) \\ & - 3(l_2 + m_2) - \cdots - N(l_{N-1} + m_{N-1})]\phi_1\} \\ & \times \exp\{i(l_1 + m_1)\phi_2\}\cdot\exp\{i(l_2 + m_2)\phi_3\}\cdot \ldots \\ & \times \exp\{i(l_{N-1} + m_{N-1})\phi_N\}]\exp\{iB\}. \end{aligned} \qquad [A21]$$

Redefining the parameters for the infinite sums,

$$\begin{aligned} l_1 + m_1 &= k_2, \\ l_2 + m_2 &= k_3, \\ &\cdots \\ l_{N-1} + m_{N-1} &= k_N, \end{aligned} \qquad [A22]$$

we get

$$\begin{aligned}D_0 = [\sum_{n=-2}^{2} b_n \sum_{k_2=-\infty}^{\infty} \sum_{k_3=-\infty}^{\infty} \cdots \sum_{k_N=-\infty}^{\infty} & J_{-n-2k_2-3k_3-\cdots-Nk_N}(-2X_1) \\ & \times J_{k_2}(-2X_2)\cdot J_{k_3}(-2X_3)\cdot \ldots \\ & \times J_{k_N}(-2X_N) \\ & \times \exp\{i(-n - 2k_2 - 3k_3 - \cdots - Nk_N)\phi_1\} \\ & \times \exp\{ik_2\phi_2\}\cdot\exp\{ik_3\phi_3\}\cdot \ldots \\ & \times \exp\{ik_N\phi_N\}]\exp\{iB\}. \end{aligned} \qquad [A23]$$

Replacing, finally, the variables X_n according to Eq. [A20] and setting the phase factor $\exp\{iB\}$ to $\exp\{iA\}$ as defined in Eq. [A12], we get the expression for D_0 given in Eq. [A14]. Herewith, the equivalence of the two approaches is established.

APPENDIX 2

NMR Spectrometer

The experiments were performed on a redesigned 300 MHz NMR spectrometer built around a wide-bore Oxford/Bruker 7 T magnet using a commercial double-resonance 4 mm MAS probehead (Chemagnetics). The modular spectrometer, shown schematically in Fig. 5, shall briefly be

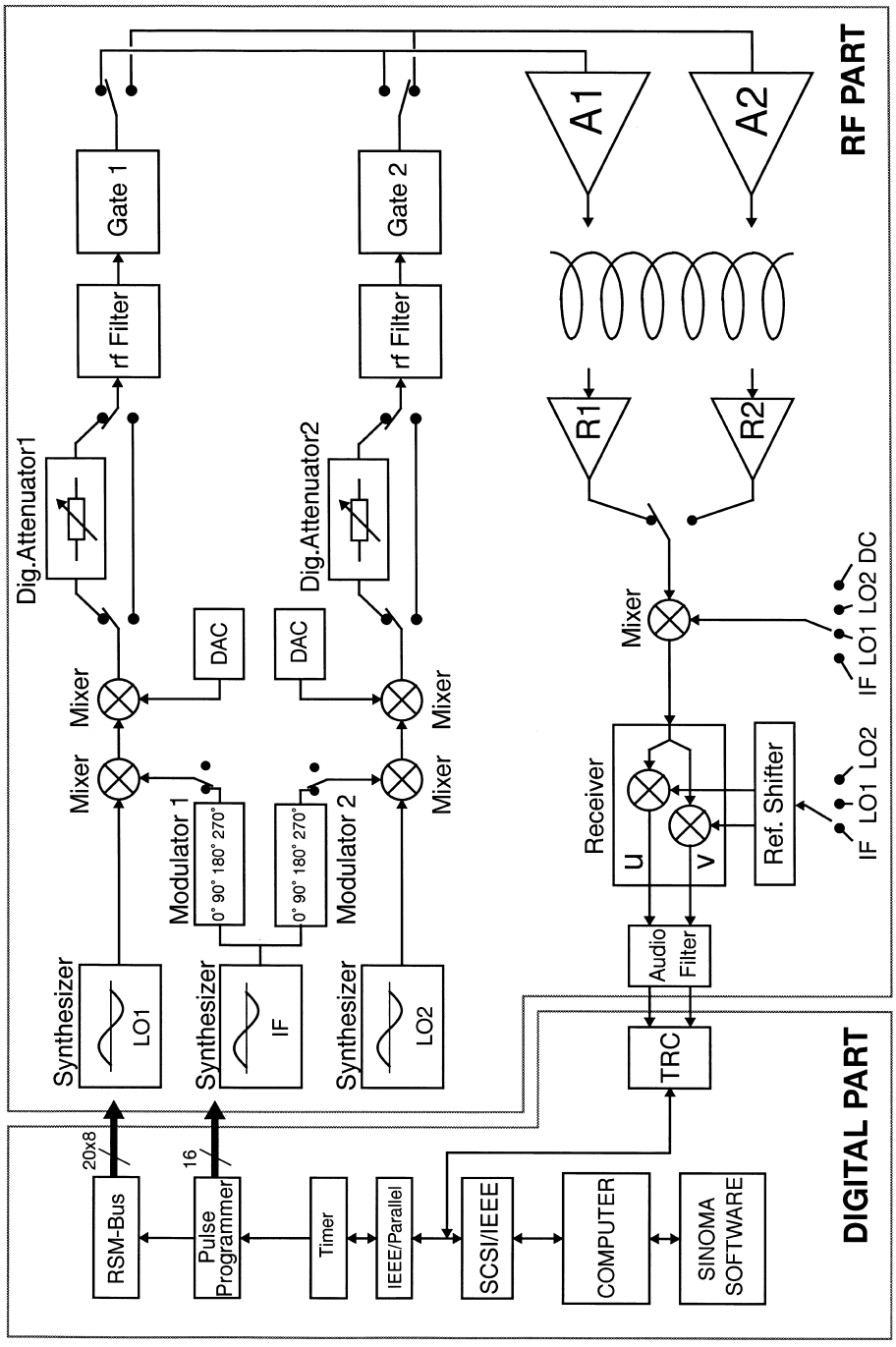

FIG. 5. Schematics of the digital and RF parts of the solid-state NMR spectrometer. The different modules are described in the text. A1 and A2 are the RF amplifiers for the two channels. R1 and R2 are the corresponding preamplifiers for the detection of the signals. TRC indicates the transient recorder.

described. It should, however, be pointed out that the experiments described in this work can be performed on modern commercial NMR spectrometers without hardware modifications.

The transmission part of the spectrometer consists of two independent, broadband RF channels with a bandwidth covering 20–300 MHz. Each of them is equipped with a fast modulator (*42*) with a switching time smaller than 20 ns between the phases 0°, 90°, 180°, and 270°, a first mixer (ZLW-1W, Mini-Circuits), a computer-controlled digital attenuator CDA0867 (DAICO Industries Inc.), a switchable RF bandpass filter (Wainwright filters for 75 or 300 MHz), and a RF gate ZFSWA-2-46 (Mini-Circuits). The shaped pulses are generated by a computer-controlled 12-bit digital-to-analog converter module (DAC, Analog Devices AD568; amplifier, Analog Devices AD840) which controls the pulse shape through a second mixer (ZLW-1W, Mini-Circuits). The input and output RF levels of all modules are set to 10 dBm. The final amplification is done by dedicated power amplifiers (Kalmus 126CRP, 200–400 MHz, 200 W, and American Microwave Technology M3200, 6–220 MHz, 1000 W). The receiver path consists of a standard Bruker preamplifier (including the proton and X-nucleus frequencies), a mixer (ZLW-1W, Mini-Circuits) to demodulate the incoming frequency, a Bruker phase-sensitive receiver, and a tunable audio filter (Rockland 452 dual hi/low filter) leading the signals to the transient recorder.

The digital part is composed of three main components: the spectrometer control computer, the pulse programmer, and the transient recorder. The computer (SGI Indy, 133 MHz R4600PC) is extended with a SCSI-IEEE488 interface (GPIB-SCSI-A with NI-488M software for IRIX5.x, National Instruments). The pulse programmer (RSM 432, 32 bit word length, Interface Technology Inc.) is interfaced to the GPIB-Bus by an IEEE-Parallel Interface (Digital488/80A, IOtech) and a specially designed timer unit allowing for real-time scan repetition. The data acquisition is performed by a transient recorder (Nicolet Pro 30: 12 bit, 10 MS/s, 256 K Memory). A special external channel advance unit had to be designed to allow for synchronous sampling of the NMR signals. This setup assures a high modularity, making it possible to exchange or modify parts of the digital section. An additional local bus, called the RSM-Bus, is connected to 16 of the 32 bits of the pulse programmer and allows, by demultiplexing, the control of 20 additional external devices, each of them driven by 8 data bits. They are used to set the frequency and the phase of the LO synthesizers PTS310 (Programmed Test Sources Inc.), as well as the computer-controlled attenuators and the DACs.

The time-event sequence of an experiment is set by the home-written package SINOMA (*43*) via a modular driver package. SINOMA provides a versatile macro language with branching and looping structures similar to C. SINOMA creates, from the user's macro, the corresponding data to load and start the RSM 432 pulse programmer. It then waits for the data, recorded in transient recorder format, to be ready and converts them to the XWIN-NMR or MATLAB format. The loop counters in SINOMA allow the performance of 1D, 2D, and 3D experiments. The experimental parameters are taken from the XWIN-NMR acquisition files. For data processing, the software packages XWIN-NMR (Bruker Analytische Messtechnik GmbH) or MATLAB (The Math Works, Inc., Massachusetts) are used.

ACKNOWLEDGMENTS

This research has been supported by the Swiss National Science Foundation. Helpful discussions with Dr. Zhehong Gan, Suzana K. Straus, Dr. Marc Baldus, and Rene Verel are acknowledged. For computer simulations, the programming environment GAMMA (*35, 36*) was used.

REFERENCES

1. S. R. Hartmann and E. L. Hahn, *Phys. Rev.* **128,** 2042 (1962).
2. A. Pines, M. G. Gibby, and J. S. Waugh, *J. Chem. Phys.* **59,** 569 (1973).
3. E. O. Stejskal, J. Schaefer, and J. S. Waugh, *J. Magn. Reson.* **28,** 105 (1977).
4. B. H. Meier, *Chem. Phys. Lett.* **188,** 201 (1992).
5. S. Ding, C. A. McDowell, and C. Ye, *J. Magn. Reson. A* **109,** 6 (1994).
6. S. Hediger, B. H. Meier, and R. R. Ernst, *Chem. Phys. Lett.* **213,** 627 (1993).
7. S. Hediger, B. H. Meier, and R. R. Ernst, *J. Chem. Phys.* **102,** 4000 (1995).
8. R. Pratima and K. V. Ramanathan, *Chem. Phys. Lett.* **221,** 322 (1994).
9. T. Gullion and J. Schaefer, *J. Magn. Reson.* **81,** 196 (1989).
10. T. Gullion and J. Schaefer, ''Detection of Weak Heteronuclear Dipolar Coupling by Rotational-Echo Double-Resonance Nuclear Magnetic Resonance,'' Vol. 13, Advances in Magnetic Resonance, Academic Press, San Diego, 1989.
11. A. W. Hing, S. Vega, and J. Schaefer, *J. Magn. Reson.* **96,** 205 (1992).
12. A. W. Hing, S. Vega, and J. Schaefer, *J. Magn. Reson. A* **103,** 151 (1993).
13. T. G. Oas, R. G. Griffin, and M. H. Levitt, *J. Chem. Phys.* **89,** 692 (1988).
14. M. H. Levitt, T. G. Oas, and R. G. Griffin, *Israel J. Chem.* **28,** 271 (1988).
15. A. E. Bennett, R. G. Griffin, and S. Vega, ''Recoupling of Homo- and Heteronuclear Dipolar Interactions in Rotating Solids,'' Vol. 33, NMR Basic Principles and Progress, Solid-State NMR IV, Springer-Verlag, Berlin, 1994.
16. K. Takegoshi, K. Takeda, and T. Terao, *Chem. Phys. Lett.* **260,** 331 (1996).
17. T. M. Barbara and E. H. Williams, *J. Magn. Reson.* **99,** 439 (1992).
18. X. Wu and K. W. Zilm, *J. Magn. Reson. A* **104,** 154 (1993).
19. B. Q. Sun, P. R. Costa, and R. G. Griffin, *J. Magn. Reson. A* **112,** 191 (1995).
20. O. B. Peersen, X. Wu, I. Kustanovich, and S. O. Smith, *J. Magn. Reson. A* **104,** 334 (1993).

21. O. B. Peersen, X. Wu, and S. O. Smith, *J. Magn. Reson. A* **106,** 127 (1994).
22. G. Metz, X. Wu, and S. O. Smith, *J. Magn. Reson. A* **110,** 219 (1994).
23. A. C. Kolbert and S. L. Gann, *Chem. Phys. Lett.* **224,** 86 (1994).
24. A. C. Kolbert and A. Bielecki, *J. Magn. Reson. A* **116,** 29 (1995).
25. H. Geen, J. J. Titman, and H. W. Spiess, *Chem. Phys. Lett.* **213,** 145 (1993).
26. S. Hediger, B. H. Meier, N. D. Kurur, G. Bodenhausen, and R. R. Ernst, *Chem. Phys. Lett.* **223,** 283 (1994).
27. S. Zhang, *J. Magn. Reson. A* **110,** 73 (1994).
28. S. Zhang, C. L. Czekaj, and W. T. Ford, *J. Magn. Reson. A* **111,** 87 (1994).
29. S. Hediger, B. H. Meier, and R. R. Ernst, *Chem. Phys. Lett.* **240,** 449 (1995).
30. M. Baldus, D. G. Geurts, S. Hediger, and B. H. Meier, *J. Magn. Reson. A* **118,** 140 (1996).
31. D. Marks and S. Vega, *J. Magn. Reson. A* **118,** 157 (1996).
32. A. Abragam, ''The Principles of Nuclear Magnetism,'' Clarendon Press, Oxford, 1961.
33. K. J. Packer and K. M. Wright, *J. Magn. Reson.* **41,** 268 (1980).
34. J. D. Crane, P. B. Hitchcock, H. W. Kroto, R. Taylor, and D. R. M. Walton, *J. Chem. Soc. Chem. Commun.* 1764 (1992).
35. S. A. Smith, T. O. Levante, B. H. Meier, and R. R. Ernst, *J. Magn. Reson. A* **106,** 75 (1994).
36. T. O. Levante, M. Baldus, B. H. Meier, and R. R. Ernst, *Mol. Phys.* **86,** 1195 (1995).
37. A. Wokaun and R. R. Ernst, *J. Chem. Phys.* **67,** 1752 (1977).
38. S. Vega, *J. Chem. Phys.* **68,** 5518 (1978).
39. R. R. Ernst, G. Bodenhausen, and A. Wokaun, ''Principles of Nuclear Magnetic Resonance in One and Two Dimensions,'' Clarendon Press, Oxford, 1987.
40. U. Haeberlen, ''High Resolution NMR in Solids, Selective Averaging,'' Vol. 1, Advances in Magnetic Resonance, Academic Press, New York, 1976.
41. M. Mehring, ''Principles of High Resolution NMR in Solids,'' 2nd ed., Springer, Berlin, 1983.
42. D. N. Shykind, G. C. Chingas, and A. Pines, *Rev. Sci. Instrum.* **61,** 1474 (1990).
43. SINOMA, *Si*gnal and *No*ise *Ma*chine, written by R. Kreis, P. Signer, and M. Tomaselli.